KRONOS FUSION ENERGY

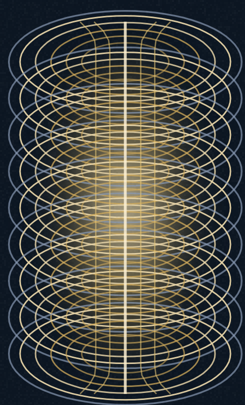

PAPER 2.16 · THE KRONOS 2026 SERIES

The Consumable Centrepost: Coverage-versus-Protection Neutronics, Coil Integrity, and Fused Quench Detection for a Compact Spherical-Tokamak Breeder

The inboard centrepost of a compact spherical-tokamak (ST) breeder sits closest to the 14 MeV source and is the machine's dominant lifetime risk: at useful breeding coverage the...

Read it live — 3-D model · physics validator · film series

BY P I FORD, R J WEGGEL AND C WEGGEL

2026 · EDITORIAL EDITION

THE OFFICIAL RECORD

What this document is, and how to read its numbers

This is a combined editorial. It gathers, in one volume, the two design studies Kronos Fusion Energy released in 2026 — a compact spherical-tokamak tritium/helium-3 breeder and a deuterium–helium-3 tandem-mirror generator — together with the intellectual-property estate, the people, and, in the internal edition, the full commercial case. The scientific text is the same text that appears in the arXiv preprints and the journal submissions; the editorial adds the apparatus a reader needs to hold the whole program at once, and nothing in the physics is altered to fit it.

THE HONESTY STANCE IS THE ASSET

Every headline quantity carries an **evidence class** — DERIVED RECOMPUTED MEASURED REQUIREMENT — and, where a number is a modelled extrapolation rather than a demonstrated value, it is labelled as such and its downside is shown next to it. Several quantities in the underlying corpus moved after first publication; where a value has been withdrawn or restated, the record says so plainly. This is deliberate: a diligence team will find the load-bearing assumptions, so the document surfaces them first.

TWO EDITIONS

This volume is issued in two editions. The **public edition** (light) carries the physics and the design only — no dollar, price, or per-kilogram figure appears anywhere in it. The **internal edition** (dark) adds the economics, the funding architecture, and the defense-commercial analysis, and is marked *Confidential* accordingly; it is not for public distribution. Where the commercial case rests on a modelled assumption rather than a demonstrated one, it is labelled as such and its downside is shown alongside it, on the same terms as the physics.

TITLE	The Kronos Fleet — Hyperion · Aegis · MetroVolt: A Combined Design & Commercialization Study
AUTHOR	Priyanca Ford, Founder & CEO, on behalf of Kronos Fusion Energy
EDITION	2026 Combined Editorial · first issue
COMPANION WORKS	The five-paper arXiv drop — (1) Breeder, (2) Burner, (3) REBCO magnet & tape, (4) Direct Energy Conversion, (5) AI/ML/Quantum control — with matching numbered Zenodo deposits, plus the IOP journal and IAEA-FEC submissions. Patents were filed before the drop.
NAMING	Hyperion = the breeder; Aegis (defense) and MetroVolt (data-center) = one generator in two housings. Internal mode letters (D1, L) do not appear on public surfaces.
STATUS	Conceptual design & simulation study. Nothing herein is a construction commitment.

HOW TO READ THIS VOLUME

The fleet at a glance, and the way its numbers are marked

This volume opens with *Orientation*, presents the five research papers as a bound sequence, and closes with the *Apparatus*. *Foundations* sets out the three general results both machines rest on. *Paper One* is the Hyperion breeder; *Paper Two* the Aegis / MetroVolt generator; *Papers Three, Four and Five* are the enabling science — high-field REBCO magnets and tape, direct energy conversion, and the AI / ML / quantum control stack. A *Digital Twin & 3-D Model* part follows, then the *Environmental* profile. The *Economics* and levelized cost and the *Business Case* and diligence record appear in the internal edition only; the *Simulations* proof record and the Apparatus — patent portfolio, team, limitations, and sources — close both editions.

THE FLEET AT A GLANCE

	HYPERION	AEGIS	METROVOLT
Role	Strategic-isotope foundry	Defense installation power	Campus power
Machine	**Spherical tokamak**	**Tandem mirror**	**Tandem mirror**
Fuel	Deuterium–tritium	Deuterium–helium-3	Deuterium–helium-3
Delivers	Tritium · ^{3}He · 14 MeV n	Resilient installation power	Firm campus power
Physics bar	**Fusion gain only**	Closure (gates named)	Closure + lunar ^{3}He
In the fleet	Breeds the fuel	Proves the generator	Commercial destination

HOW THE NUMBERS ARE MARKED

Every headline quantity carries an evidence class — DERIVED from first principles, RECOMPUTED from raw data, MEASURED in hardware, or a REQUIREMENT yet to be met. Financial figures carry a case label and are confined to the internal (confidential) edition. Values that moved after first publication are shown as withdrawn or restated rather than quietly changed. A capability you can evaluate is one whose limits are on the page.

ABSTRACT

The Consumable Centrepost: Coverage-versus-Protection Neutronics, Coil Integrity, and Fused Quench Detection for a Compact Spherical-Tokamak Breeder

The inboard centrepost of a compact spherical-tokamak (ST) breeder sits closest to the 14 MeV source and is the machine's dominant lifetime risk: at useful breeding coverage the high-temperature REBCO conductor reaches its irradiation limit in a small fraction of a full-power year (fpy). We treat the centrepost as a *consumable, scheduled-replacement* cartridge and quantify the architecture through four coupled analyses on the frozen Hyperion design point (configuration 22021, $\delta = -0.30$, $B_0 = 8\,\mathrm{T}$, centrepost peak field $16.84\,\mathrm{T}$). Casting the inboard radial budget as a constrained optimisation, a three-dimensional OpenMC scan of the $72\,\mathrm{cm}$ inboard-column split (tungsten-carbide shield versus beryllium-multiplied breeding mantle) yields the coverage-versus-protection Pareto set: net tritium breeding ratio (TBR) falls monotonically from 1.196 to 1.097 as the shield grows from 5 to $40\,\mathrm{cm}$, while centrepost life at the Fischer REBCO onset threshold ($3.9 \times 10^{22}\,\mathrm{n\,m^{-2}}$) rises from 0.0048 to $0.194\,\mathrm{fpy}$ — the binding constraint is centrepost life, not breeding. The damage and cryogenic heat load fall with the shield at e-folding lengths of ~ 11 and $\sim 9\,\mathrm{cm}$ respectively, and the life obeys an exact iso-elastic mission-dial law (life $\times$ source $=$ const) that carries a $2.25\times$ margin to the $6.57\,\mathrm{MA}$ mid-current point. A wedged-sector finite-element model reproduces the analytic thick-wall (Lam\'e) bore hoop stress to -4.75% (625.3 versus $656.6\,\mathrm{MPa}$). A fused strain-rate-plus-magnetization quench detector triggers at $0.089\,\mathrm{s}$ against $3.024\,\mathrm{s}$ for voltage detection — a protection lead of $2.935\,\mathrm{s}$ inside a $3.672\,\mathrm{s}$ MIITs budget, at fused signal-to-noise 322.5; an in-winding nitrogen-vacancy (NV) diamond magnetometer supplies the magnetization channel with a functional-life margin of $39\times$ over one cartridge life. A reliability/availability (RAMI) model of the demountable-cartridge swap gives a plant availability of 0.5825 for a dedicated outage, rising to 0.5904 when swaps are merged with scheduled maintenance — honestly below a continuous-duty reference. Together the analyses convert a lifetime showstopper into a scheduled maintenance line item with a quantified cadence and a quantified availability cost. No net-electricity claim is made: Hyperion is a breeder and materials platform, and these results describe how it survives its own neutron environment.

Open-access deposit (code & data, CC BY 4.0): DOI 10.5281/zenodo.22645704 · Zenodo community *kronos_fusion_energy*. Explore it live: interactive 3-D model · physics validator.

Keywords: spherical tokamak centrepost REBCO magnet neutronics quench detection tritium breeding availability negative triangularity

CONTENTS

Table of Contents

NOMENCLATURE

Symbols, units, and the names of things

Q	plasma (fusion) gain, P_{fus}/P_{aux}
Q_E	engineering gain, net electric out / recirculating in
H_{98}	confinement enhancement over the IPB98(y,2) scaling
Z_{eff}	effective ion charge
c_{ee}	electron–electron bremsstrahlung leading coefficient, 2.120022 (exact)
τ_E	energy confinement time
I_p	plasma current
R_0, a	major radius, minor radius
κ, δ	elongation, triangularity
β_N	normalized plasma beta (Troyon-normalized)
TBR	tritium breeding ratio
DEC	direct energy conversion
CF	plant capacity factor (availability)
FOAK / NOAK / BOAK	first / n^{th} / best of a kind
Hyperion	the ST breeder (internal: Mode D2)
Aegis	the generator, defense/installation housing (internal: Mode M)
MetroVolt	the generator, data-center housing (Mode M)

spherical tokamak; centrepost; REBCO magnet; neutronics; quench detection; tritium breeding; availability; negative triangularity

Nomenclature tocsectionNomenclature

@L>X@ SYMBOL	DEFINITION
t_{sh}	tungsten-carbide inboard-shield thickness (cm); scan variable trading breeding coverage against centrepost protection
TBR	net tritium breeding ratio on the 14.06 MeV spectrum
fpy	full-power year, 3.156×10^{7} s
$\Phi(\quad r)$	fast-neutron fluence ($E > 0.1$ MeV) accumulated at the conductor
Φ_{lim}	REBCO fast-fluence critical-current onset threshold, $3.9 \times 10^{22}\,\mathrm{n\,m^{-2}}$ (Fischer)
τ_{cp}	centrepost life to the fluence limit (fpy)
S_n	volumetric 14 MeV neutron source strength ($\mathrm{s^{-1}}$)
σ_θ	azimuthal (hoop) stress in the centrepost conductor (MPa)
J	mean current density in the centrepost conductor ($\mathrm{A\,m^{-2}}$)
MIITs	$\int I^2\,\mathrm{d}t$ adiabatic quench-protection budget ($\mathrm{MA^2\,s}$)
z_S, z_M, z_F	strain-rate, magnetization, and fused quench-precursor window statistics
NV	nitrogen-vacancy diamond magnetometer (in-winding sensor)
A **(RAMI)**	steady-state plant availability

§ 1

Introduction

THE CENTREPOST IS THE LIFETIME PINCH-POINT

The spherical tokamak (ST) confines a large plasma current in a small volume behind a slim inboard column, which is precisely what makes it an attractive compact neutron source and breeder platform [1,2,3]. The same slimness places the centrepost conductor in the most intense fast-neutron field in the device. The Hyperion breeder holds $I_p = 9.66$ MA at a major radius of only $R_0 = 1.20$ m behind a centre-post magnet whose peak field is 16.84 T, in a negative-triangularity ($\delta = -0.30$) regime chosen for its quiescent, edge-localised-mode-free edge [6,7]. For a high-temperature REBCO centrepost, the critical-current onset threshold under fast fluence is reached in a small fraction of a full-power year, so treating the centrepost as a permanent component is not credible for a 14 MeV breeder. Neutron irradiation of REBCO coated conductor degrades the critical current well before it damages the plasma- facing structure [12,13]; the magnet, not the wall, is the first thing to die.

We therefore adopt a *consumable-centrepost* architecture — a demountable, scheduled-replacement inboard cartridge, in the same spirit as the demountable-magnet ARC concept [3] — and answer four questions on the frozen design point. *(i)* How does inboard shielding trade against breeding coverage? *(ii)* Does the coil survive its own Lorentz loads? *(iii)* Can a quench be caught fast enough to protect a no-insulation winding? *(iv)* What maintenance cadence and plant availability does the swap imply? The contribution of this paper is to answer all four quantitatively, on one frozen configuration, with the neutronics, structural, protection, and availability analyses coupled through a single inboard radial budget, and to show that the answers convert a lifetime showstopper into a scheduled maintenance line item.

PRIOR ART AND THE DESIGN CONTEXT

Neutron shielding of an ST centre column is an established but unresolved design tension. Windsor and co-workers showed that tungsten borides outperform monolithic tungsten as centre-column shields by roughly an order of magnitude in flux and heating attenuation [19,18], and the general shielding-versus- build tension for compact STs is well documented; the residual problem is that shielding the magnet steals radial space from the breeding blanket. Tritium breeding at net TBR above unity is itself a demanding requirement for a compact machine [23,5], and the coupling between shield thickness and breeding coverage is exactly the trade this paper quantifies. On the magnet side, no-insulation (NI) REBCO technology underlies recent record fields [8,9] and compact high-field tokamak concepts [4,3,11], but its slow normal-zone propagation makes quench detection a genuine protection liability [24], motivating the non-voltage, fused-sensor detector developed here [25,26]. Damage accumulation and transmutation in the surrounding structure are quantified with the standard NRT displacement metric [20] and integrated materials- response models [21,22], and the neutron transport itself rests on modern Monte-Carlo methods with evaluated data [14,15] and global variance reduction [17].

RELATION TO THE KRONOS SERIES AND SCOPE

This paper is a companion to the Hyperion breeder platform [31] and shares its configuration and neutronics basis. It sits at the hub of a cluster of companion results: the deeper fast-fluence/dpa life-limiter analysis [33], the source-strength-versus-life operating-window synthesis [34], the first-principles radiation tolerance of centrepost REBCO [35], the REBCO high-field conductor basis [36], the net-blanket-TBR fleet case [40], the dedicated fused NV-diamond quench- detection study [37], the demountable-cartridge swap-logistics and fleet-RAMI models [38], and the distinct 26.49 T burner plug coil [39] — a separate, higher-field magnet that must never be conflated with the 16.84 T breeder centrepost. Throughout, *no net-electricity claim is made*: Hyperion is a breeder and strategic-materials platform, and the results below describe only how it survives its own neutron environment. Every headline quantity is a frozen anchor in the Kronos Physics De-Risking Register [32], and the register gate identifiers (e.g. BR-L1-A13b) are given inline so each number is auditable.

§ 2

Governing equations and the formal problem

THE COVERAGE-VERSUS-PROTECTION PROBLEM

The inboard column has a fixed radial budget. Axis outward, it is built as a homogenised Cu/SS316 conductor ($r < 20$ cm), a tungsten-carbide shield of thickness t_{sh}, and the beryllium-multiplied breeding mantle. With a 72 cm column and a 20 cm conductor, the mantle build is $47 - t_{sh}$ (in cm), so the shield and the mantle compete one-for-one: every centimetre of protection is a centimetre of lost breeding coverage. The design problem is therefore a scalar constrained optimisation over the single variable t_{sh},

$$\max_{t_{sh}} \tau_{cp}(t_{sh}) \qquad \text{s.t.} \qquad \text{TBR}(t_{sh}) \geq \text{TBR}_{min}, \quad t_{sh} \in [t_{min}, 47\ \text{cm}],$$

where τ_{cp} is the centrepost life and TBR_{min} is the breeding floor set by the fuel-cycle requirement. Both objective and constraint are monotone but opposed in t_{sh} (life rises, TBR falls), so the solution lives on the Pareto boundary; the engineering choice is where on that boundary to sit. The remainder of this section derives $\text{TBR}(t_{sh})$ and $\tau_{cp}(t_{sh})$ from transport, the coil stress from elasticity, the protection lead from the quench heat balance, and the availability from a renewal model.

NEUTRON TRANSPORT, FLUENCE, AND LIFE

The angular flux $\psi(\mathbf{r}, \boldsymbol{\Omega}, E)$ obeys the steady linear Boltzmann transport equation,

$$\boldsymbol{\Omega}\cdot\nabla\psi + \Sigma_t(\mathbf{r}, E)\,\psi = \int_{4\pi}\int_0^\infty \Sigma_s(\mathbf{r}, E' \to E, \boldsymbol{\Omega}'\cdot\boldsymbol{\Omega})\,\psi(\mathbf{r}, \boldsymbol{\Omega}', E')\,\mathrm{d}E'\,\mathrm{d}\boldsymbol{\Omega}' + \frac{S_n(\mathbf{r})}{4\pi}\chi(E),$$

with macroscopic total and scattering cross-sections Σ_t, Σ_s and a monoenergetic 14.06 MeV D–T source of strength S_n and spectrum $\chi(E) = \delta(E - 14.06\,\text{MeV})$. Two functionals of the solution close the problem. The net tritium breeding ratio integrates the $^6\text{Li}(n, \alpha)t$ and $^7\text{Li}(n, n'\alpha)t$ reaction rates over the mantle and normalises to the source,

$$\text{TBR} = \frac{1}{S_n}\int_{V_{mantle}}\int_0^\infty \left[\Sigma_6(\mathbf{r}, E) + \Sigma_7(\mathbf{r}, E)\right]\phi(\mathbf{r}, E)\,\mathrm{d}E\,\mathrm{d}V,$$

with $\phi = \int_{4\pi}\psi\,\mathrm{d}\boldsymbol{\Omega}$ the scalar flux. The fast-fluence rate at the conductor is the $E > 0.1$ MeV flux, and the centrepost life is the Fischer onset threshold divided by that rate,

$$\dot{\Phi}_{fast}(\mathbf{r}) = \int_{0.1\,\text{MeV}}^\infty \phi(\mathbf{r}, E)\,\mathrm{d}E, \qquad \tau_{cp} = \frac{\Phi_{lim}}{\max_{r\in V_{cp}} \dot{\Phi}_{fast}(\mathbf{r})}, \qquad \Phi_{lim} = 3.9 \times 10^{22}\,\text{n}\,\text{m}^{-2}.$$

Because equations (3)–(4) are ratios of flux to source, both TBR and the flux-per-source are pure functions of geometry: they do not depend on the absolute source strength. This is the origin of the *iso-elastic mission-dial law*. Writing the operating source strength as S_n and holding the geometry fixed, the fluence rate scales linearly with S_n and the life scales inversely,

$$\dot{\Phi}_{fast} \propto S_n \quad \Longrightarrow \quad \tau_{cp}(S_n)\,S_n = \text{const.}$$

Hence the same geometry that yields the design-point life at $I_p = 9.66$ MA yields exactly $\tau_{cp} \times (S_n^{des}/S_n^{mid})$ at the reduced 6.57 MA mid-current point; the frozen ratio is 2.25. The displacement-damage rate follows the same geometry-only scaling through the NRT kernel [20],

$$\dot{d}_{dpa}(\mathbf{r}) = \frac{1}{N}\int_0^\infty \phi(\mathbf{r}, E)\left[\int_0^\infty \sigma(E, T)\,\nu_{NRT}(T)\,\mathrm{d}T\right]\mathrm{d}E, \qquad \nu_{NRT} = \frac{0.8\,T_{dam}}{2E_d},$$

with N the atom density, $\sigma(E, T)$ the recoil cross-section, T_{dam} the damage energy and E_d the displacement threshold; the resulting $\dot{d}_{dpa}$ and the volumetric nuclear heating both attenuate quasi-exponentially through the shield.

REBCO CRITICAL-CURRENT DEGRADATION AND THE FLUENCE LIMIT

The threshold in equation (4) is a property of the conductor, not of the geometry. Fast-neutron irradiation introduces point defects and cascade damage in the REBCO layer, and the in-field critical current I_c falls with accumulated fluence. Over the operationally relevant range the degradation is well described by an initial plateau followed by a near-exponential decline,

$$\frac{I_c(\Phi)}{I_c(0)} = \exp\big[-(\Phi/\Phi_0)^m\big], \qquad \Phi_{\text{lim}} \equiv \Phi \text{ at } I_c/I_c(0) = 1 - \eta_c,$$

where Φ_0 and the stretch exponent m are fitted to reactor-irradiation data and η_c is the tolerable critical-current loss. Taking the Fischer onset value $\Phi_{\text{lim}} = 3.9 \times 10^{22}\,\text{n}\,\text{m}^{-2}$ [12] as the retirement criterion is conservative: it is the fluence at which the in-field I_c first departs measurably from its unirradiated value, well before the steep part of equation (7). The first-principles basis of Φ_{lim} — chain-oxygen-vacancy formation and displacement cascades in YBCO — is developed in the companion radiation-tolerance study [35]; here it enters only as the scalar retirement fluence.

COIL STRUCTURAL INTEGRITY: THE LAM\'E HOOP-STRESS BOUND

The centrepost carries the toroidal-field current at the smallest radius in the machine, so its structural limit is set by its own self-field body force rather than by any external load. For an axisymmetric conductor of outer radius a carrying total current I at mean current density $J = I/\pi a^2$, Amp\`ere's law gives the enclosed azimuthal field $B_\theta(r) = \mu_0 J r/2$, and the Lorentz body force density is radial and inward-compressing,

$$f = \quad J \times \quad B = - \quad \hat{} \; r \, \frac{\mu_0 J^2 r}{2}.$$

Treating the conductor as a thick-walled cylinder in equilibrium, the radial and azimuthal (hoop) stresses obey the elasticity balance $\mathrm{d}\sigma_r/\mathrm{d}r + (\sigma_r - \sigma_\theta)/r + f_r = 0$ closed by the plane-strain compatibility relation [30]. Integrating with a traction-free outer surface and a solid core yields the classical Lam\'e-type solution whose peak is the membrane hoop stress at the bore,

$$\sigma_\theta^{\max} = \frac{\mu_0 J^2 a^2}{4}\, g(\nu), \qquad g(\nu) = \frac{3+\nu}{4} + (\text{winding-pack correction}),$$

with ν the effective Poisson ratio of the winding pack and $g(\nu)$ an $O(1)$ Poisson/geometry factor. The monotone radial profile — peak at the bore, falling outward — identifies the bore membrane hoop stress as the single binding structural quantity, and equation (9) is the closed-form target that the finite- element model must reproduce (§4.4).

QUENCH HEAT BALANCE, THE MIITS BUDGET, AND FUSED DETECTION

A no-insulation REBCO centrepost has a large temperature margin but a very slow normal-zone propagation velocity, so a developing hot spot can reach a damaging temperature before it generates a measurable resistive voltage [24]. In the adiabatic hot-spot limit the local energy balance equates Joule heating to the enthalpy rise of the conductor,

$$J(t)^2\, \rho(T) = \gamma\, C_p(T)\, \frac{\mathrm{d}T}{\mathrm{d}t},$$

with electrical resistivity ρ, mass density γ and specific heat C_p. Separating variables and integrating from the operating temperature T_{op} to a material limit $T_{\max}$ defines the protection budget in the MIITs (mega-amp-squared-seconds) form,

$$\int_0^{t_q} I(t)^2\, \mathrm{d}t = A_{\text{cond}}^2 \int_{T_{\text{op}}}^{T_{\max}} \frac{\gamma\, C_p(T)}{\rho(T)}\, \mathrm{d}T \equiv \text{MIITs},$$

where A_{cond} is the conductor cross-section; the frozen budget is $3.672\,\text{MA}^2\,\text{s}$. A detector must fire while the accumulated $\int I^2 \mathrm{d}t$ is safely below this bound. We fuse two non-voltage precursor channels: a fibre-Bragg *strain-rate* statistic z_S reading the mechanical signature of local current redistribution [25], and a *magnetization* statistic z_M reading the collapse of the screening current [26]. Each is a matched-template z-score over the precursor window. Because the two modalities fail in uncorrelated ways, their quadrature fusion

$$z_F = \frac{z_S + z_M}{\sqrt{2}}, \qquad \text{SNR}_F^2 = \text{SNR}_S^2 + \text{SNR}_M^2,$$

carries a window statistic whose signal-to-noise ratio adds the single-channel ratios in quadrature. The detection lead is the difference between the fused trigger time and the voltage-detection time, and must be positive with margin inside the MIITs budget of equation (11).

AVAILABILITY OF A SCHEDULED-SWAP CARTRIDGE

Because the centrepost has a finite life τ_{cp}, the plant alternates between an uptime interval $T_{up} = \tau_{cp}$ and a swap downtime T_{sw}. In the renewal (alternating-process) model the steady-state availability is

$$A = \frac{\text{MTBF}}{\text{MTBF} + \text{MTTR}} = \frac{T_{up}}{T_{up} + T_{sw}} \cdot \Pi_{other},$$

where $\Pi_{other} < 1$ folds in all other scheduled and unscheduled outages. Merging the centrepost swap with an otherwise-scheduled maintenance window removes the swap's dedicated contribution to the denominator: if a fraction β of the swap downtime overlaps existing outages, the effective downtime is $T_{sw}(1-\beta)$, which is the single largest controllable lever on A. Equations (1)– (13) are the formal problem; the rest of the paper evaluates them on the frozen configuration.

§ 3

Computational methodology: the NVIDIA GPU HPC campaign

Every quantity in this paper was produced on the Kronos NVIDIA GPU HPC campaign — Kronos-owned A100/H100-class clusters for offline multi-physics Monte-Carlo and structural sweeps, with bare-metal nodes for deterministic, jitter-free integration of the protection and availability models. The campaign runs the full neutron-transport and structural sweeps that recompute the breeding and centrepost-integrity envelopes; the same frozen result set is re-derivable from the open register deposit. Four solvers were run for this paper.

NEUTRON TRANSPORT (OPENMC)

The coverage-versus-protection trade (gate BR-L1-A13b) was computed with OpenMC 0.15.3 [14] on the FENDL-3.2 fusion library, with cross-check runs on ENDF/B-VIII.0 [15]. The geometry is the validated coupled three-dimensional build — elliptical plasma/SOL/first-wall/blanket/vessel tori at $R_0 = 120$ cm, $a = 48$ cm, $\kappa = 2.0$ — with the inboard column resolved, axis outward, as homogenised Cu/SS316 conductor ($r < 20$ cm), the tungsten-carbide shield of thickness t_{sh}, and the beryllium-multiplied breeding mantle ($f_{\text{Be}} = 0.80$, ^{6}Li enrichment 0.90). A uniform 14.06 MeV D–T volume source drives the transport of equation (2). The estimators of equations (3)–(6) are tallied on a cylindrical mesh over the inboard column. *Variance reduction.* Because the conductor sits deep behind the shield, an analogue random walk starves the tally; we generate MAGIC weight windows [17] from a first coarse pass and apply them on a cylindrical mesh, cutting the conductor fast-flux relative error to 0.01–0.03 at 4×10^5 source particles. *Convergence and verification.* The full-machine tally (gate BR-L1-A5, 1.2×10^8 histories) closes the neutron balance to leakage 0.121 and reproduces the calibration anchor bit-consistently: net TBR 1.0537, conductor fast flux 6.21×10^{11} n cm^{-2} s^{-1}, and life 0.199 fpy at the reference split. The mid-to-design life ratio 2.25 matches the iso-elastic law of equation (5) exactly, an independent check on the source normalisation. A CAD-faithful STEP-to-DAGMC pathway reproduces the same net TBR in the companion neutronics study [42].

COIL FINITE-ELEMENT MODEL

The bore hoop stress of equation (9) was solved (gate 02) with a wedged-sector finite-element model of the inner turn: a periodic angular sector of the winding pack under the self-field body force of equation (8), plane-strain in the axial direction, with an effective winding-pack Poisson ratio and traction-free outer boundary. The mesh is refined toward the bore, where the membrane hoop stress peaks; convergence is declared when the bore stress changes by $< 0.5\%$ under a further halving of the element size. The solution is verified against the closed-form Lam\'e bound as an analytic manufactured reference (§4.4).

QUENCH TRANSIENT AND DETECTOR STATISTICS

The adiabatic hot-spot integral of equations (10)–(11) was integrated (gate 03) with temperature-dependent $\rho(T)$, $C_p(T)$ on the frozen conductor cross-section to give the temperature trajectory $T(t)$ and the MIITs budget 3.672 MA^2 s. The fused-detector statistics of equation (12) were evaluated on the modelled precursor transient, returning the channel trigger times and the fused signal-to-noise. The in-winding NV-diamond magnetometer that supplies the magnetization channel is specified and its neutron functional-life margin computed in the dedicated companion study [37]; here the sensor enters through the frozen $39\times$ life margin.

RAMI MONTE-CARLO

The availability of equation (13) was evaluated (gate 04) with a time-domain reliability model of the demountable-cartridge swap: uptime intervals set by τ_{cp}, swap downtime distributions, and an overlap fraction β for the merge with scheduled maintenance. The dedicated-versus-merged availability figures follow directly; the full fleet-level time-domain Monte-Carlo across a four-unit breeder fleet is developed in the companion RAMI study [38].

§ 4

Results

THE COVERAGE-VERSUS-PROTECTION TRADE

Table 2 gives the trade curve at the design point with the breeding mantle on, and figure 1 plots it. Net TBR falls monotonically from 1.196 (5 cm shield) to 1.097 (40 cm) as centrepost life at the Fischer threshold rises from 0.0048 to 0.194 fpy. The mantle-off reference ($f_{\text{in}} = 0$) gives net TBR 1.053 at life 0.206 fpy. The trade is steep and binding: no split simultaneously delivers a high TBR and a multi-year centre-post, which is precisely why the consumable frame is the right one. The design picks a breeding-favourable split and absorbs the life as a scheduled swap. Figure 2 shows the same data as the breeding-versus-life Pareto set; the operating choice is a point on this boundary, not a compromise off it.

t_{sh} (CM)	MANTLE (CM)	NET TBR	LIFE 1E22	LIFE 3.9E22	LIFE 1E23	DPA/FPY	HEAT (W)
5	42	1.196	0.0012	0.0048	0.012	0.412	937
10	37	1.193	0.0018	0.0071	0.018	0.264	563
15	32	1.188	0.0029	0.0115	0.029	0.164	337
20	27	1.181	0.0051	0.0198	0.051	0.094	185
25	22	1.170	0.0086	0.0336	0.086	0.056	112
30	17	1.154	0.0155	0.0606	0.155	0.031	61
35	12	1.130	0.0279	0.109	0.279	0.018	36
40	7	1.097	0.0496	0.194	0.496	0.010	20
ref (f_{in}=0)	17	1.053	0.053	0.206	0.527	0.010	18

Centrepost coverage-versus-protection trade at the 9.66 MA design point, breeding mantle on. Life columns are at the 1×10^{22}, 3.9×10^{22} (Fischer), and $1 \times 10^{23}\,\text{n}\,\text{m}^{-2}$ thresholds; mid- current (6.57 MA) lives are 2.25× the design values at every split (equation 5). Source: gate BR-L1-A13b, `cp_split_scan_results.json`.

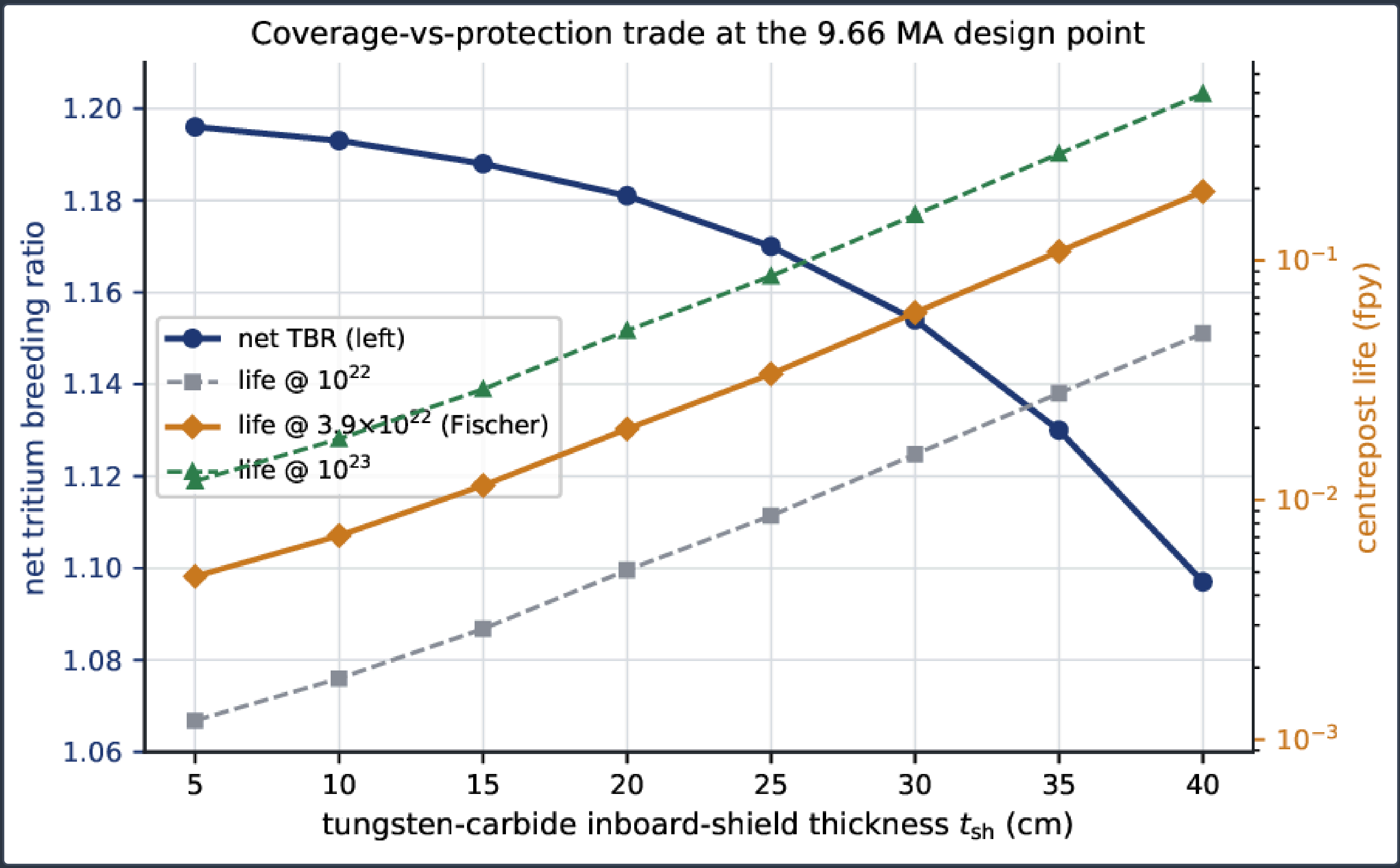

Coverage-versus-protection trade at three fluence thresholds (gate BR-L1-A13b): net TBR (navy, left) falls monotonically as the tungsten-carbide shield thickens, while centrepost life (right, logarithmic) rises. The amber diamonds are the Fischer onset threshold ($3.9 \times 10^{22}\,\mathrm{n\,m^{-2}}$), the binding retirement criterion.

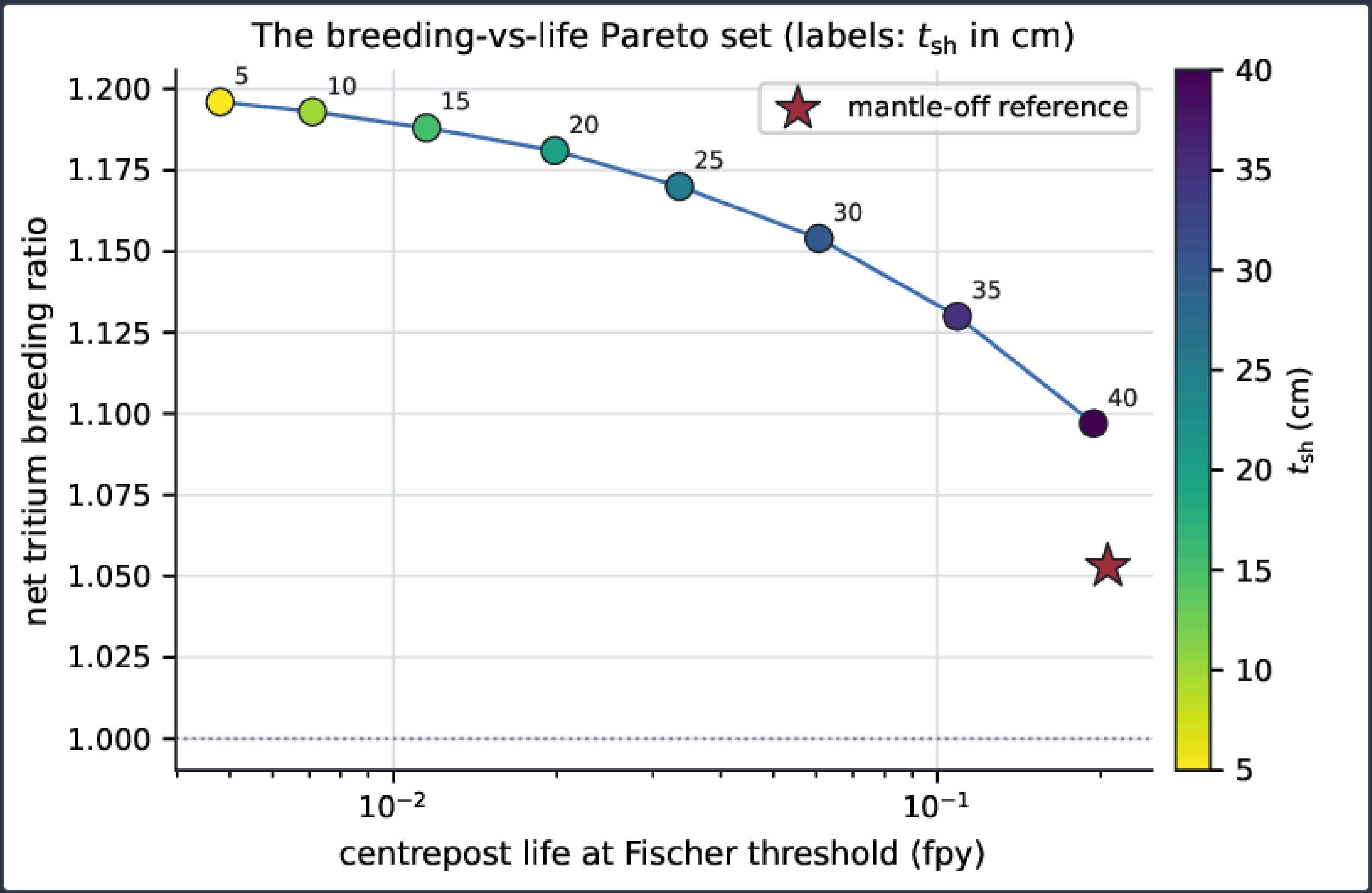

The breeding-versus-life Pareto set from Table 2; marker colour and label give the shield thickness t_{sh} (cm), the abscissa is centrepost life at the Fischer threshold (logarithmic), and the red star is the mantle-off reference. Every attainable operating point lies on this frontier.

SHIELD EFFECTIVENESS: DAMAGE AND CRYOGENIC HEAT

The shield does more than protect the critical current: it attenuates the displacement-damage rate of equation (6) and the volumetric nuclear heating that the cryoplant must remove. Figure 3 shows both falling quasi-exponentially with t_{sh}, with e-folding lengths of ~ 11 cm for the damage rate and ~ 9 cm for the heating. Across the scan the damage rate falls from 0.412 to 0.010 dpa/fpy and the centrepost nuclear heating from 937 to 20 W — a factor of ~ 47 in the cold- mass heat load, which is the coupling into the cryogenic budget quantified in the companion cold-mass study [43]. The shield choice is therefore a three-way coupling of breeding, magnet life, and refrigeration load, all resolved on the single variable t_{sh}.

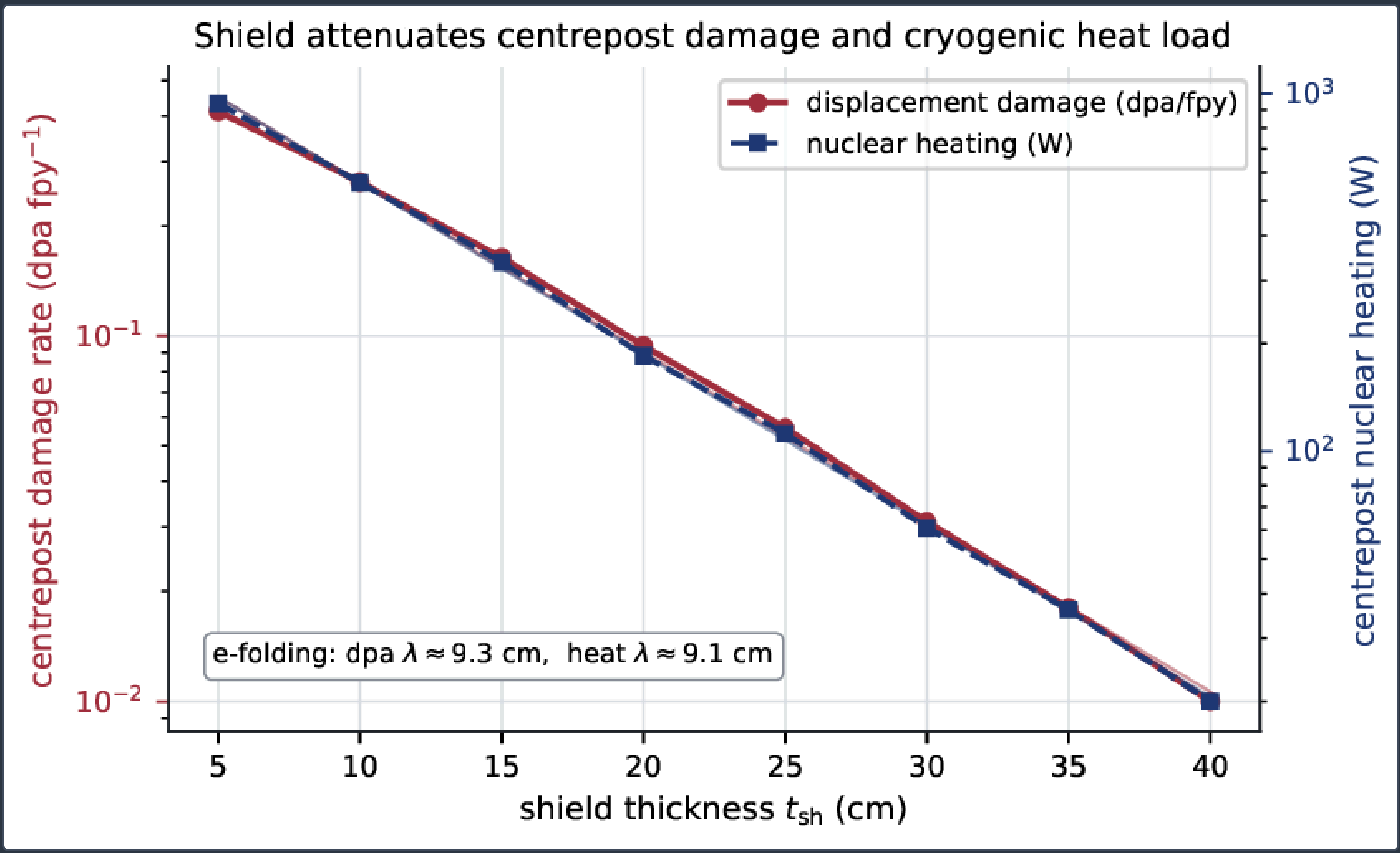

Shield attenuation of centrepost displacement damage (red, dpa/fpy) and nuclear heating (navy, W) versus t_{sh}; both axes are logarithmic and the faint lines are single-exponential fits with the quoted e-folding lengths. The heat curve is the coupling into the cryogenic budget (gates BR-L1-A13b, BR-L1-A13).

THE ISO-ELASTIC MISSION DIAL

Equation (5) makes the life a geometry-only quantity scaled by the inverse source strength. Figure 4 plots the Fischer-threshold life for the **9.66** MA design point and the **6.57** MA mid-current point, which differ everywhere by the exact factor **2.25**. At the most-shielded end of the trade — a full **45** cm tungsten-carbide shield — the best-case cartridge life reaches **0.58 fpy**, the scheduled- replacement design point. The mission dial is thus a genuine operational lever: derating the current (or, more precisely, the source strength) buys centrepost life on a one-for-one inverse basis, and the admissible current window that results from folding this against the source-strength requirement is the subject of the companion operating-window synthesis [34].

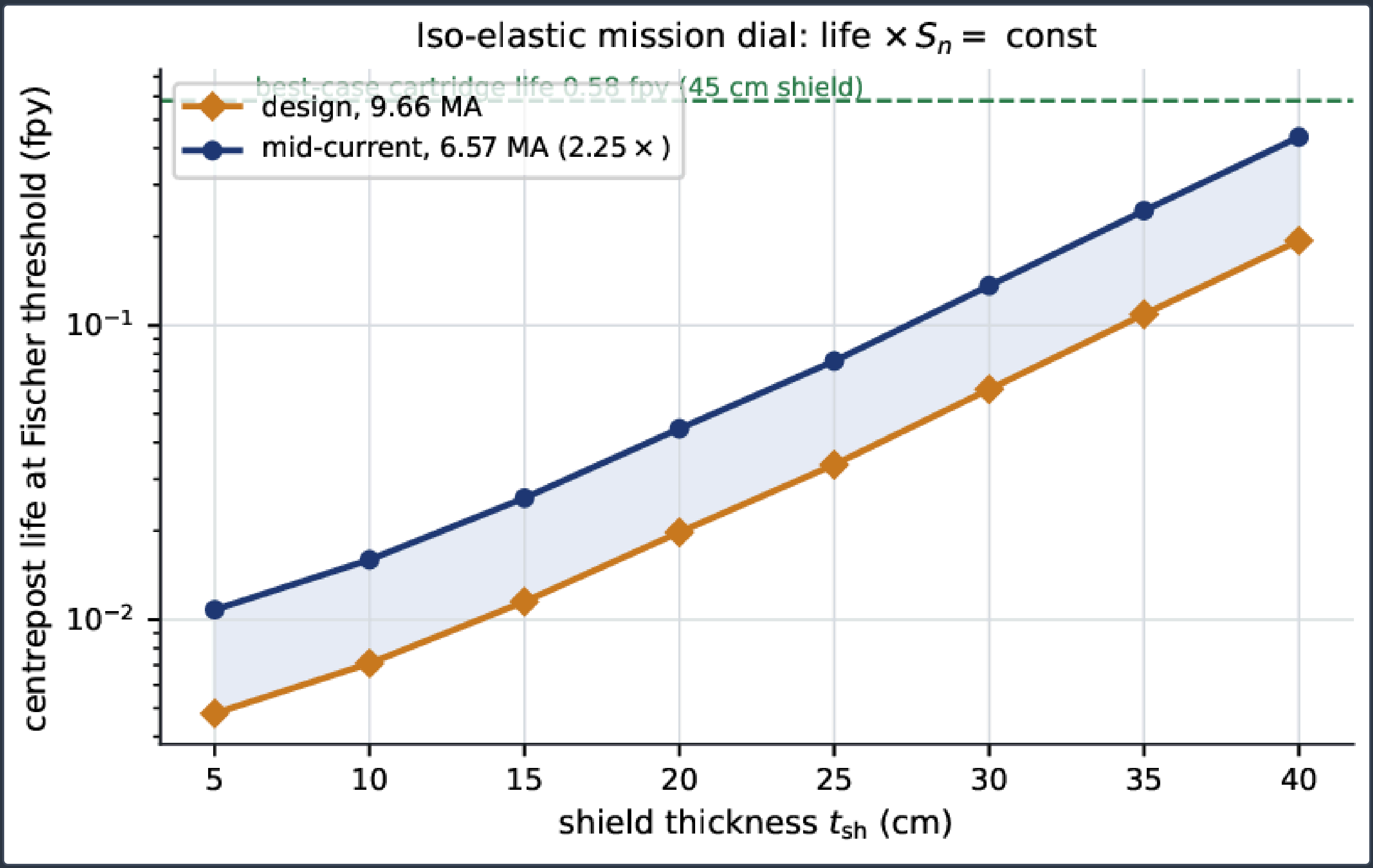

Iso-elastic mission dial (equation 5): centrepost life at the Fischer threshold for the design (**9.66** MA) and mid-current (**6.57** MA) points, separated everywhere by the exact factor **2.25**. The dashed line marks the best-case **0.58 fpy** cartridge life at the fully shielded (**45** cm) end.

COIL STRUCTURAL INTEGRITY

Evaluated on the as-built centrepost, the closed-form bound of equation (9) gives a bore membrane hoop stress of **656.6** MPa, and the wedged-sector finite-element solution gives **625.3** MPa — a difference of −**4.75**%. Figure 5 plots the full radial profile: the finite-element and Lam\'e curves track each other across the whole bore-to-outer span, peaking at the bore and falling monotonically outward, and agreeing to within a few per cent everywhere. The agreement verifies the reduced-order structural model and confirms the membrane hoop stress as the binding structural quantity. The monotone profile motivates a per-turn engineered residual pre-compression that flattens the Lorentz strain gradient — the mechanical companion to the neutronics-driven swap cadence, and consistent with the structural mechanics of the surrounding vessel support [44].

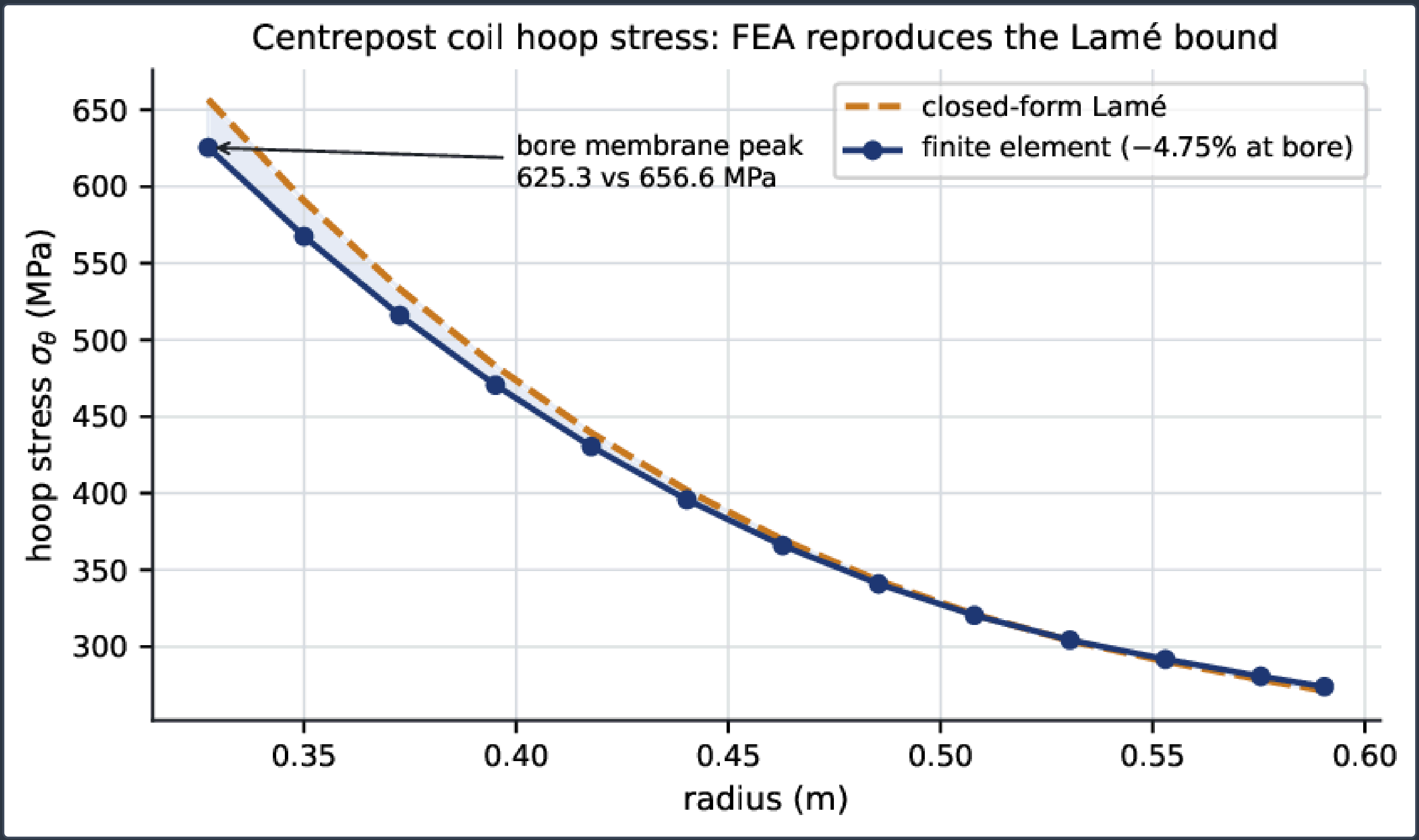

Bore-resolved centrepost coil hoop stress: wedged-sector finite element (navy) versus the closed-form Lam\'e thick-wall bound (amber, equation 9), agreeing to −**4.75**% at the bore membrane peak (**625.3** versus **656.6** MPa; gate 02). The shaded band is the FEA–analytic difference.

QUENCH PROTECTION AND FUSED DETECTION

Integrating the adiabatic hot-spot balance of equations (10)–(11) gives the conductor temperature trajectory of figure 6. The fused strain-rate-plus-magnetization detector triggers at **0.089** s, when the conductor has reached only **47** K, whereas conventional voltage detection does not fire until **3.024** s, at **174** K. The protection lead is **2.935** s, comfortably inside the **3.672** s MIITs budget, and the fused window statistic reaches a signal-to-noise of **322.5**. Figure 7 shows why fusion wins: the strain-rate and magnetization channels carry window-statistic signal-to-noise of **2.00** and **2.78**, and their quadrature combination (equation 12) yields **3.43** — a strictly larger statistic than either channel, with the earliest trigger time. The magnetization channel is supplied by an in-winding NV-diamond magnetometer whose coherence survives the alpha environment; fast-neutron creation of NV centres sets a functional-life requirement that is met with a factor-**39** margin over one cartridge life (**0.22 fpy** design, **0.496 fpy** mid-current), the same margin carried in the dedicated NV-quench study [37].

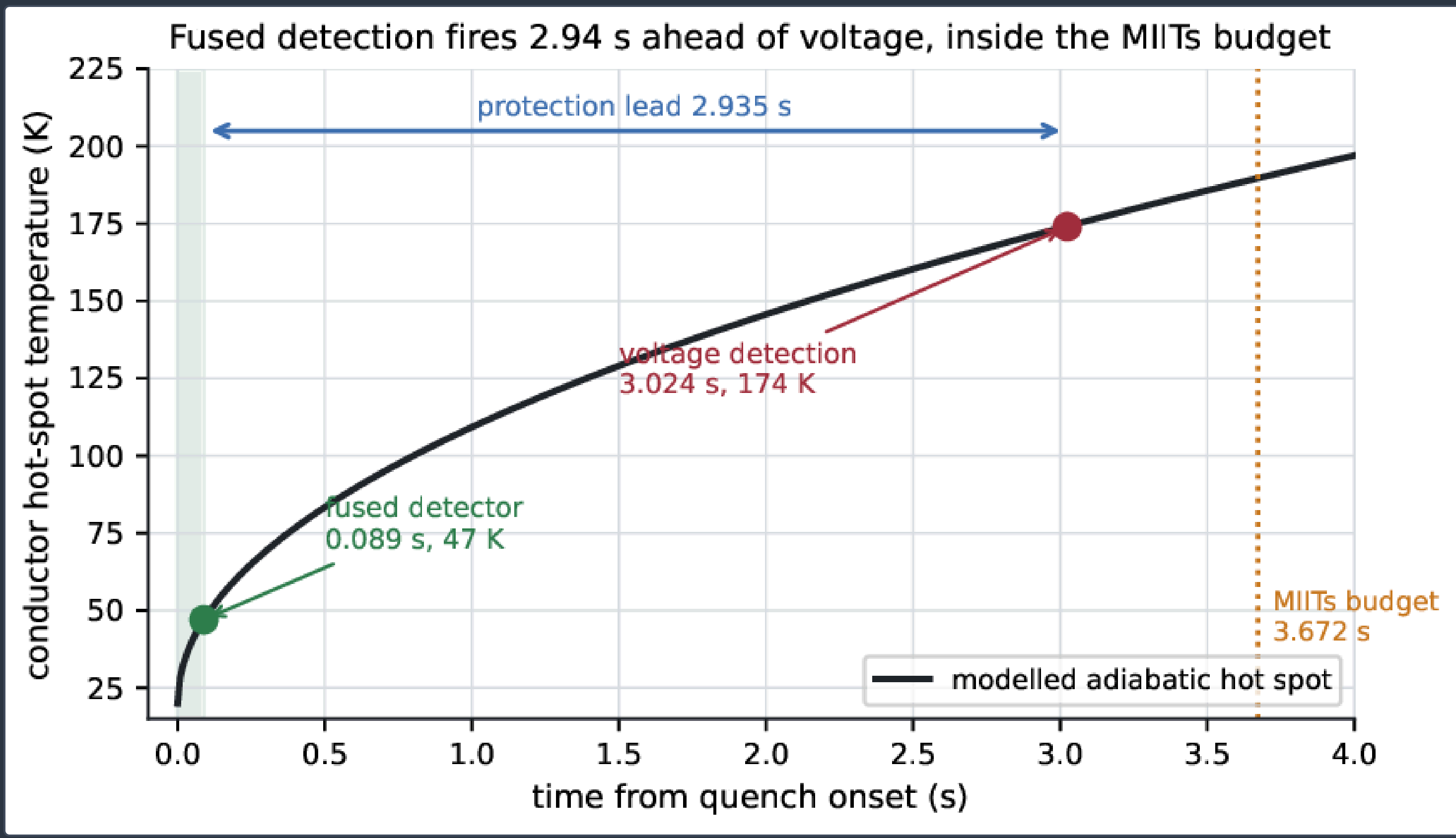

Modelled adiabatic hot-spot temperature trajectory (equations 10–11; gate 03). The fused detector fires at **0.089** s / **47** K (green), voltage detection at **3.024** s / **174** K (red); the protection lead of **2.935** s sits inside the **3.672** s MIITs budget (amber). The connecting curve is the model; the two detection points are the frozen results.

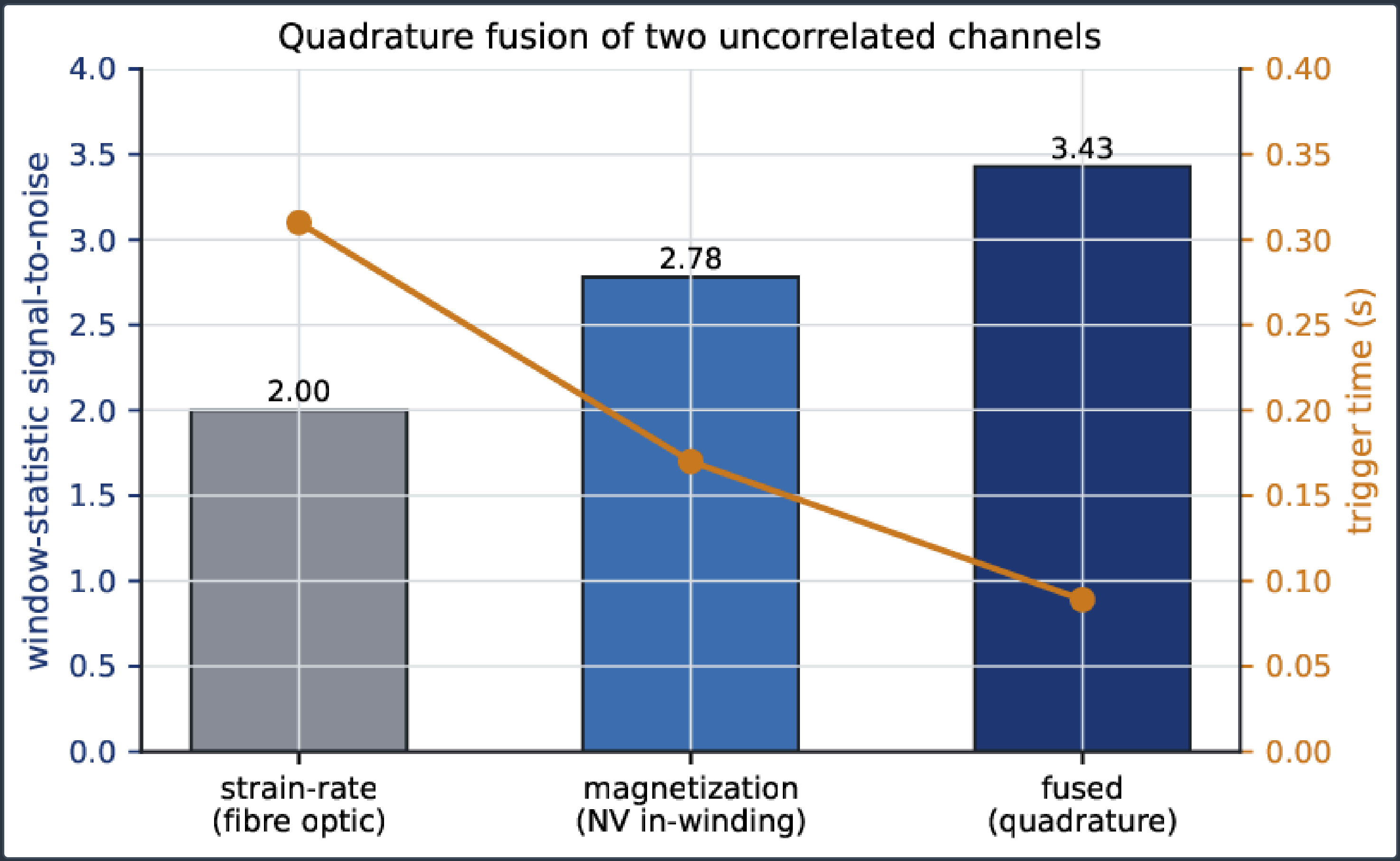

Quadrature fusion of two uncorrelated precursor channels (equation 12; gate 03): window- statistic signal-to-noise for the strain-rate, magnetization, and fused channels (bars, left axis) and their modelled trigger times (amber, right axis). Fusion produces both the largest statistic and the earliest trigger.

MAINTENANCE CADENCE AND AVAILABILITY

The demountable cartridge turns the finite centrepost life into a swap schedule. Evaluating the renewal model of equation (13) on the frozen swap logistics gives a plant availability of **0.5825** when the centrepost swap is a dedicated outage, rising to **0.5904** when swaps are merged with otherwise-scheduled maintenance (figure 8). At the longer mid-current cadence the same model gives **0.6382** (dedicated) and **0.6477** (merged). We report this honestly: all four figures sit below a conventional continuous-duty reference (capacity factor **0.69**), and the merge — removing the swap's dedicated contribution to the downtime denominator — is the single largest controllable lever on availability. Availability, not breeding, is the line item that the consumable-centrepost architecture must manage; the fleet-level time-domain treatment across a four-unit breeder fleet is the subject of the companion RAMI study [38].

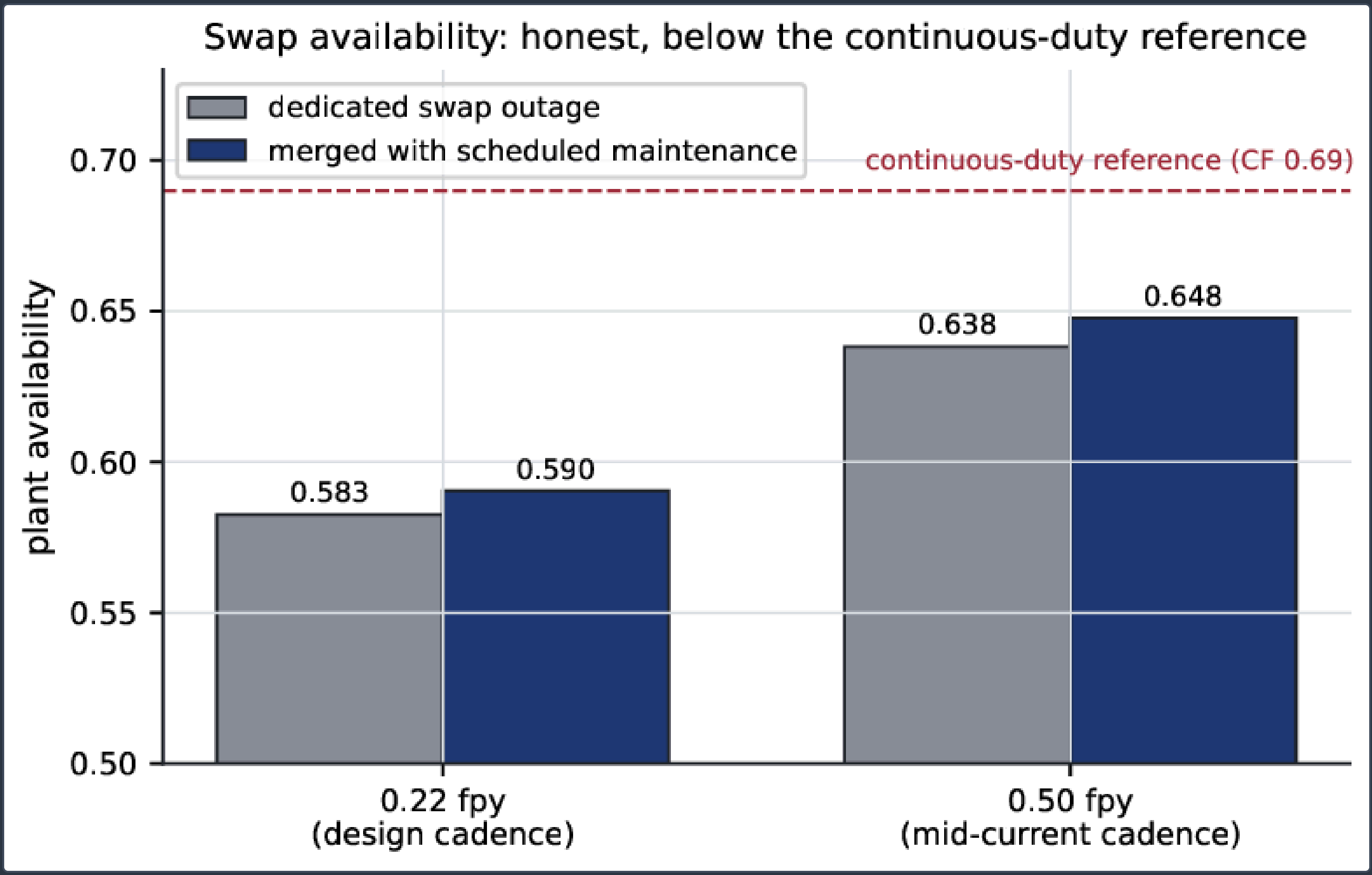

Plant availability from the renewal model (equation 13; gate 04): dedicated swap outage (grey) versus merge with scheduled maintenance (navy), at the design (**0.22 fpy**) and mid-current (**0.50 fpy**) cadences. All figures sit honestly below the continuous-duty reference (dashed, CF **0.69**).

THE ARCHITECTURE, ASSEMBLED

Figure 9 is the radial-build schematic that ties the four analyses together: the conductor, the scan-variable shield, and the breeding mantle share one 72 cm inboard column, and figure 10 is the fused-detection architecture that protects it. Together they realise the consumable-centrepost concept — a demountable cartridge whose life is set by neutronics, whose structure is verified against a closed form, whose quench is caught by a fused non-voltage detector, and whose swap is costed in availability.

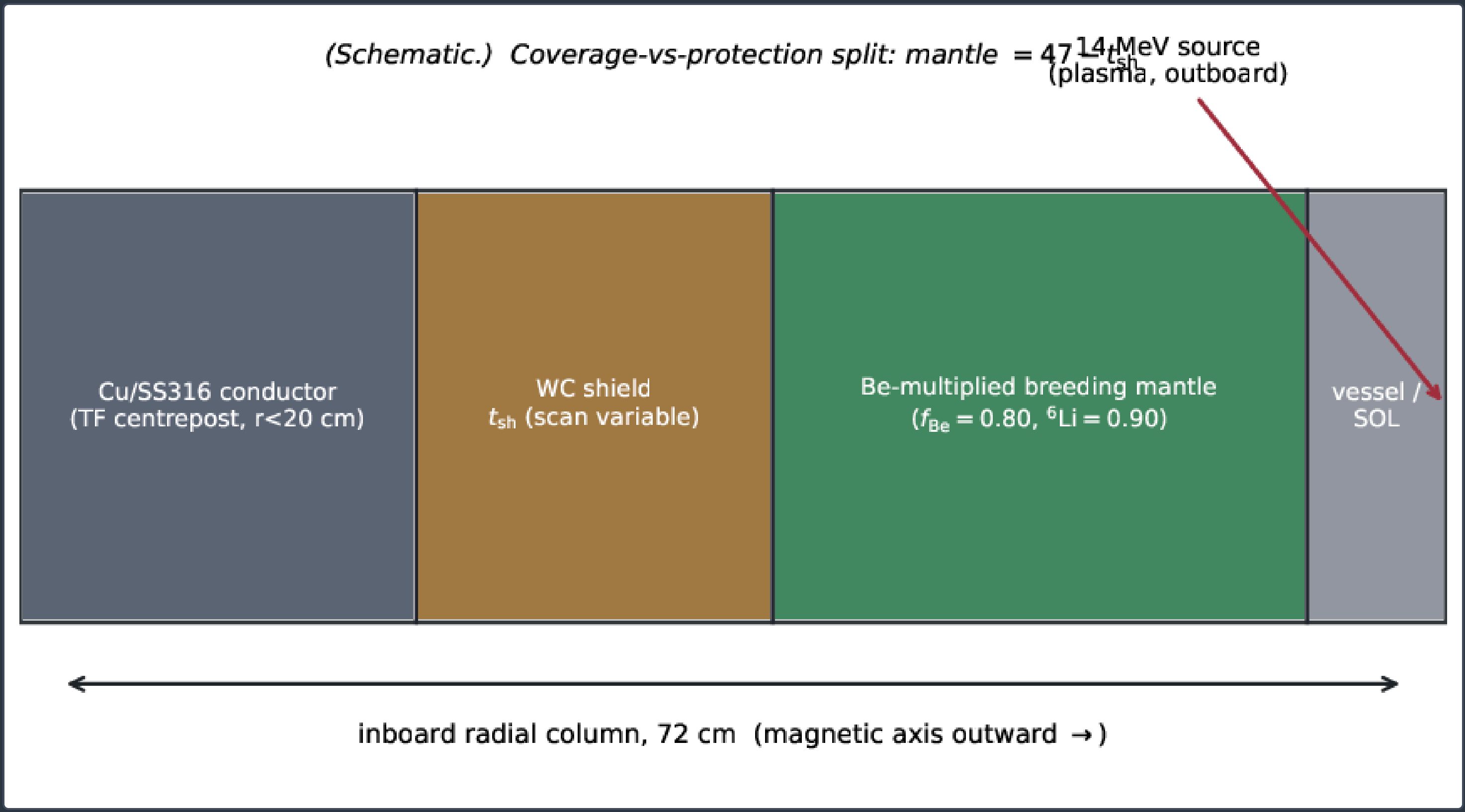

(Schematic.) The consumable-centrepost inboard radial build: Cu/SS316 conductor ($r < 20$ cm), tungsten-carbide shield of scan-variable thickness t_{sh}, and beryllium-multiplied breeding mantle ($47 - t_{sh}$), sharing one 72 cm column with the 14 MeV source outboard. No data values are shown; the figure encodes the coverage-versus-protection split only.

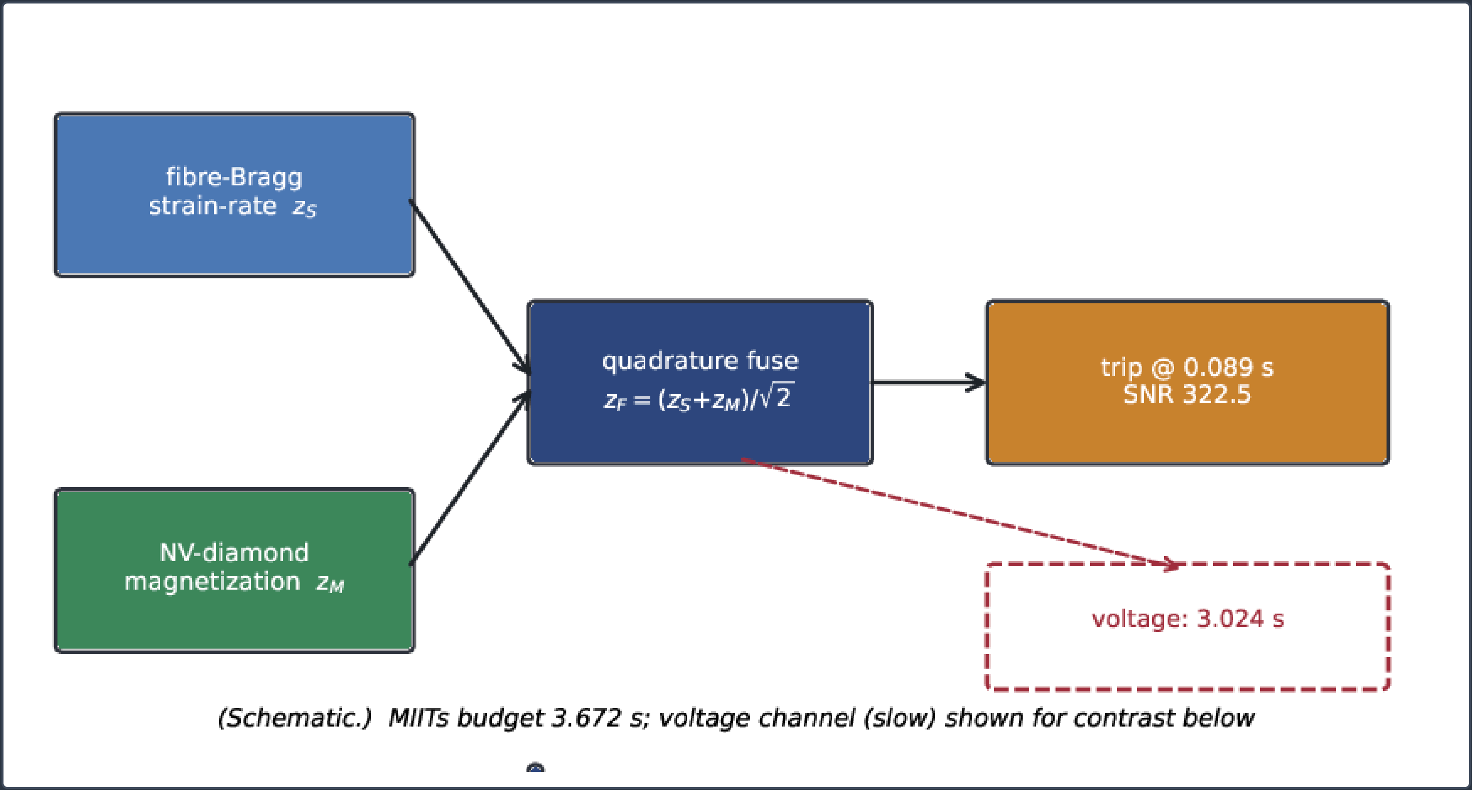

(Schematic.) The fused quench-detection architecture: a fibre-Bragg strain-rate channel and an in-winding NV-diamond magnetization channel are combined in quadrature (equation 12) to trip at 0.089 s, far ahead of the slow voltage channel (3.024 s). Structure only; the numeric labels are the frozen detection results.

§ 5

Discussion

The four analyses close a consistent picture, and each admits a quantitative comparison with the published literature.

Shielding and breeding. Our tungsten-carbide centre-column shield attenuates the conductor fast flux strongly enough that the binding constraint becomes centrepost life rather than breeding, exactly the regime Windsor and co-workers identified for tungsten-boride shields in a compact ST, where flux and heating are cut by about an order of magnitude relative to bare tungsten [19,18]. Our net TBR stays above unity across the entire scan (1.097–1.196), which places the machine on the self-sufficient side of the breeding requirement documented for compact DEMO-class systems [23,5]; the fleet-level tritium export case rests on the same net-TBR result [40,41]. The steepness of the trade — a $\sim 40\times$ swing in life for a $\sim 8\%$ swing in TBR — is what forces the consumable frame: there is no split that is simultaneously breeding-rich and long-lived.

The REBCO fluence limit. The Fischer onset threshold of $3.9 \times 10^{22}\,\mathrm{n\,m^{-2}}$ [12] that sets the retirement criterion is consistent with the broader reactor-irradiation literature on coated conductors, which reports heavy in-field critical-current degradation and transition-temperature suppression at fluences of this order [13]. Adopting the *onset* of degradation rather than a fractional-loss criterion is deliberately conservative and keeps the design well up the plateau of equation (7); the first-principles justification — oxygen-vacancy formation energies and displacement cascades in YBCO — is developed in the companion radiation-tolerance study [35], and the conductor and stabiliser materials response under irradiation in the conductor-materials study [36].

Coil structure. The -4.75% agreement between the wedged-sector finite element and the closed-form Lam\'e bound (equation 9) is well within the tolerance expected for a homogenised-winding-pack membrane calculation, and the bore-peaked monotone profile matches the classical thick-wall solution [30]. The 625.3 MPa bore stress is a large but manageable membrane load for a stainless- steel-reinforced winding pack, consistent with the structural envelopes reported for high-field REBCO magnets [8,11]. Crucially, the breeder centrepost governs at 16.84 T; it is a distinct device from the separate 26.49 T burner plug coil [39], and the two must never be conflated.

Quench detection in context. The fused detector should be read against the slow-normal-zone-propagation problem that motivates it. Marchevsky's review makes the core point quantitatively: in HTS conductors the large temperature margin and slow propagation mean a hot spot can reach damaging temperature before a measurable resistive voltage appears, so voltage detection alone is inadequate [24]. The community response has been non-voltage observables: Salazar *et al.* demonstrated fibre-Bragg thermometry on VIPER cable at SULTAN with signal-to-noise of 4–32 for heater-induced events [25], and Teyber *et al.*\ showed current-distribution monitoring detecting quench and damage in fusion cables [26]. Our contribution is complementary: fusing an uncorrelated strain-rate and magnetization pair (equation 12) lifts the window statistic above either channel and buys a 2.935 s protection lead inside the MIITs budget — early, low-false-alarm warning in the low-signal corner the slow-propagation physics forces a real magnet into. The picotesla-class sensitivity of the in-winding NV magnetometer sits well inside the envelope established for ensemble NV magnetometry [27,28,29], so the sensing claim rests on a conservative device with large margin for multiplexing and in-service degradation.

Availability. The reported availabilities (0.5825–0.6477) are honestly below a continuous-duty reference, and we do not dress them up. The value of the analysis is that it makes the availability penalty of the consumable centrepost *explicit and controllable*: the merge lever recovers roughly one percentage point, and the mid-current cadence lever recovers several more, both of which are quantified against the same renewal model [38]. This is the standard RAMI posture for maintenance-limited fusion systems [5], applied to a component whose finite life is treated as a scheduled interval rather than a failure.

§ 6

Limitations

The results are design-and-simulation on the frozen configuration, not measurements from an operating machine. The one open engineering item is the in-winding NV sensor's neutron tolerance: the analytical sensor sensitivity assumes an ensemble coherence and contrast that will degrade under the high background field, cryogenic operation, and fast-neutron creation of NV centres in the diamond. The mitigation is quantified — the functional-life requirement is met with a factor-**39** margin over one cartridge life, and the fused detector retains its precursor advantage with the NV channel heavily degraded — but a dedicated NV neutron-tolerance study (irradiation plus first-principles charge-state modelling) is the follow-on that closes it [37]. Beyond that, the homogenised conductor composition and the wedged-sector mechanical model are reduced representations of a real winding pack; the fused-detector lead margin is computed for a modelled transient and awaits bench confirmation on real REBCO; and the availability figures depend on swap-logistics assumptions stated with the model rather than measured. The neutronics carry Monte-Carlo statistics (relative error **0.01–0.03**) and the Fischer threshold is a retrieved onset value, not a device-specific measurement.

§ 7

Conclusion

Treated as a consumable, the centrepost stops being a showstopper. On the frozen Hyperion design point the coverage-versus-protection trade is steep and binding — net TBR 1.196 to 1.097 against Fischer-threshold life 0.0048 to $0.194\,\mathrm{fpy}$ across the shield scan — so the design chooses breeding coverage and absorbs the life as a scheduled swap, with the damage rate and cryogenic heat load attenuated by $\sim 40\times$ and $\sim 47\times$ respectively and the life obeying an exact iso-elastic mission-dial law with a $2.25\times$ margin to mid-current. The coil matches its analytic hoop stress to -4.75%, a fused strain-rate-plus- magnetization detector leads voltage detection by 2.935 s inside the 3.672 s MIITs budget at signal-to-noise 322.5, and the swap costs availability (0.5825–0.6477) that the merge with scheduled maintenance partly recovers. The centrepost's finite life becomes a maintenance line item with a quantified cadence, not a barrier to a compact ST breeder. Hyperion is a breeder and materials platform; these results describe how it survives its own neutron environment.

Acknowledgments tocsectionAcknowledgments Part of the Kronos Fusion Energy 2026 design series. The authors thank the Kronos physics de-risking programme for the frozen result set underlying every quantitative claim, and the NVIDIA GPU HPC campaign that produced the neutron-transport, structural, quench, and availability results.

Reproducibility. Every headline quantity in this paper is a frozen anchor in the Kronos Physics De-Risking Register [32] (doi:10.5281/zenodo.22133057): the coverage-versus-protection scan (gate BR-L1-A13b), the full-machine neutron balance (BR-L1-A5), the neutron-damage rate (BR-L1-A13), the coil finite- element regression (gate 02), the fused-detector timeline (gate 03), and the RAMI availability (gate 04). Each is regenerable from the archived solvers and the figure-generation script deposited with this paper; this paper is archived at doi:10.5281/zenodo.22645704; official version: https://www.kronosfusionenergy.com/publications/centrepost-and-magnet-integrity.html. No result depends on unpublished or proprietary data.

Scope — what this paper does not claim. The centrepost life is a scheduled-replacement interval, not a claim of a long-lived component; the availability figures are engineering projections, not operating data; and no net-electricity claim is made.

Data availability tocsectionData availability The trade curve, the shield-attenuation series, the coil hoop-stress profile, the quench transient, and the RAMI figures used for figures 1–8 are archived with the deposit at doi:10.5281/zenodo.22645704, which references the Kronos 2026 series including the breeder platform [31] and the De-Risking Register [32]. Headline quantities are regenerable by named scripts (`cp_split_scan.py`, `centrepost_fea.py`, `quench_analysis.py`) that read their inputs from a declared-parameter table. All quantitative values trace to the register by the gate identifiers cited inline. Any economic analysis is reported separately and is not part of the public deposit.

Competing interests tocsectionCompeting interests Provisional patent applications relating to aspects of this work have been filed.

tocsectionReferences

APPARATUS

Portfolio, People & Record

The intellectual-property estate, the people who built it, the limitations that gate it, and the sources it rests on.

1	4	40	27
GRANTED PATENT	2026 PROVISIONALS	TEAM MEMBERS	2022 PROVISIONALS

INTELLECTUAL PROPERTY

The patent portfolio

The estate spans a granted high-field magnet patent, pending utility and 2026 provisional filings that map to the two products, a digital-twin control provisional, a registered trademark application, and the original 2022 provisional family. Every patentable disclosure in the five-paper arXiv drop was protected **before** publication: the breeder and burner provisionals were filed 1–2 August, and a publication-gap omnibus filing the evening before the drop swept up the DEC, plasma-control, and REBCO-winding matter of the three otherwise-unprotected papers. Patent numbers and application serials are matters of public record; claim scope is summarised, not reproduced.

GRANTED & PENDING UTILITY

US 12,009,112	High-field tilted graded-REBCO magnet architecture (KRONO-002A) · *app. 17/878,550*	GRANTED
US 17/878,507	Core device / method (KRONO-001A) · *utility*	PENDING

2026 PROVISIONAL FILINGS — MAPPED TO THE PRODUCTS

64/124,209	Hyperion — spherical-tokamak tritium / helium-3 foundry · *breeder · filed Aug 2026*	FILED
64/124,220	Aegis / MetroVolt — synchrotron-cutoff, fuel-selection & plug-winding · *generator · filed Aug 2026*	FILED
64/115,167	KRONOS-CTRL digital-twin plant control · *provisional · filed Jul 2026*	FILED
64/005,440	Integrated spherical-tokamak fusion architecture · *early integrated-architecture filing · filed Mar 2026*	FILED
64/105,530	Negative-triangularity spherical-tokamak architecture · *foundational ST filing · filed Jul 2026*	FILED
64/128,097	Publication-gap omnibus — quasineutral two-species expander DEC · provenance-gated / latency-split plasma control · as-built high-field winding & conductor architecture · *filed 7 Aug 2026, the evening before the arXiv drop*	FILED

TRADEMARK & ORIGIN

FTK-98801894	Kronos Fusion Energy — trademark application	FILED
KR-2022-*	Original provisional family (KR-2022-00001 … 00027) · *27 filings, 2022*	PRIORITY

The narrow, defensible magnet novelty — the specific conductor and the digital-twin winding optimisation, not high-field REBCO as a category — is the commercial core that can earn ahead of any Q > 1 milestone, with markets in fusion magnet supply, MRI/NMR, accelerators, and proton therapy. The claim is scoped honestly: the high field is a *system field* result, not a stand-alone-coil record; the small-bore plug coil is structurally infeasible as a bare winding but resolved by a stress-managed structural shield (feasible-pending-FEA); and the winding-tape experiment returned a *null result*. The value is the method, not a field record.

THE TEAM

Founding partners, board, advisors & auditors

Kronos is built by a bench of advanced-fuel-fusion, high-field-magnet, direct-conversion, and materials specialists, with a board and operations team drawn from defense, national laboratories, and industry. Dates are shown as ranges; where a tenure has ended or is term-ending, the range says so.

FOUNDING PARTNERS — SCIENCE

Dr. Gerald Kulcinski
Co-Founder · Helium-3 & Advanced-Fuel Fusion
UW–Madison · 2023–Present

Dr. Carl Weggel
Chief Scientist / S.M.A.R.T. Design
MIT Alcator Program · 2022–Present

Dr. Robert J. Weggel
Magnetic Field Design
MIT Magnet Lab · 2022–Present

BOARD

Priyanca Ford
Founder & CEO · Executive Board
2022–Present

Bandel Carano
Finance / Strategy
Oak Investment Partners / Stanford · 2025–2026

Patrick Schweiger
Fusion Device Engineering
Oklo / CFS / TerraPower · 2025–Present

SCIENTIFIC ADVISORS

Dr. Steven O. Dean
Fusion Policy & History
DOE / Fusion Power Associates · 2025–Present

Dr. Patrick H. Diamond
Plasma Turbulence & Transport
UC San Diego · 2025–Present

Dr. Jack J. Dongarra
HPC & Numerical Algorithms
Turing Award · 2025–Present

Dr. Nasr M. Ghoniem
Chief Material Scientist
UCLA · 2025–Present

Dr. Siegfried Glenzer
Plasma Physics & Laser Fusion
Stanford / SLAC · 2022–Present

Dr. David A. Hammer
Pulsed-Power Fusion
Cornell · 2025–Present

Dr. Donald A. Spong
Plasma Theory & Confinement
ORNL · 2025–Present

Dr. Curtis Smith
Risk Assessment & Nuclear PRA
MIT / Idaho National Lab · 2025–Present

RADM (Ret.) David Goggins
Naval Engineering & Power-Plant Design
U.S. Navy · 2023–2026

Dr. Konstantin Batygin
Mathematician
Caltech · 2022–2025

Dr. Ruben Fair
Magnet Design / ITER Liaison
PPPL / Jefferson Lab · 2022–2025

Dr. Paul S. Weiss
Materials & Nanotechnology
UCLA · 2022–2025

SCIENTIFIC AUDITORS

Dr. Wilfred A. Cooper
Plasma Equilibrium Theory
EPFL / Swiss Plasma Center · 2025–Present

Dr. Ahmed Hassanein
Plasma–Material Interactions
Purdue / Argonne · 2025–Present

Dr. Patrick E. Hopkins
Extreme Thermal Materials
U. of Virginia · 2025–Present

Dr. Peter Hosemann
Materials Joining & Structural Integrity
UC Berkeley · 2025–Present

Dr. Travis W. Knight
Advanced Nuclear Fuels & Systems
U. of South Carolina · 2025–Present

Dr. Philippe Lebrun
Cryogenics & Magnet Cooling
CERN · 2025–Present

Dr. Nitendra Singh
Nuclear Safety & Fuel Cycle
ITER · 2025–Present

Dr. Guido Van Oost
Magnetic Confinement & Fusion Systems
Ghent University · 2025–Present

Dr. Gary S. Was
Radiation Materials & Structural Integrity
U. of Michigan · 2025–Present

Dr. Ray Sedwick
Direct Energy Conversion
U. of Maryland · 2025

OPERATIONS

Michael Laughlin
Chief Operating Officer
2022–Present

Martin Owens
Chief Strategy Officer
LANL / GE Hitachi · 2022–Present

MG (Ret.) Paul Pardew
Chief Contracting Officer
Army Contracting Command · 2022–Present

David Beck
Fusion Commercialization
U.S. Space Force · 2024–Present

Sushma Bhatia
Environmental & Legislative
Google · 2022–Present

Michael De Frenza
Technology Licensing
2023–Present

MG (Ret.) Robin L. Fontes
Cybersecurity & Defense
Army Cyber Command · 2022–Present

Vijay Gehani
Supply Chain & Components
INOX India · 2024–Present

Jon Michel Greenwood
IT & AI Infrastructure
Live Nation · 2023–Present

Brian C. O'Neill
National Security
CIA / ODNI · 2022–Present

Gen. (Ret.) Gustave F. Perna
DoD Liaison
Operation Warp Speed · 2022–2023

Andrea Romero
Marketing Lead
2022–Present

Legal counsel is retained; those roles are held on the internal roster and are not listed here.

SOURCES

References

1 J E Menard *et al*, Fusion nuclear science facilities and pilot plants based on the spherical tokamak, *Nucl. Fusion* **56** 106023 (2016). doi:10.1088/0029-5515/56/10/106023

2 J E Menard *et al*, Prospects for pilot plants based on the tokamak, spherical tokamak and stellarator, *Nucl. Fusion* **51** 103014 (2011). doi:10.1088/0029-5515/51/10/103014

3 B N Sorbom *et al*, ARC: a compact, high-field, fusion nuclear science facility and demonstration power plant with demountable magnets, *Fusion Eng. Des.* **100** 378 (2015). doi:10.1016/j.fusengdes.2015.07.008

4 A J Creely *et al*, Overview of the SPARC tokamak, *J. Plasma Phys.* **86** 865860502 (2020). doi:10.1017/S0022377820001257

5 G Federici *et al*, Overview of the DEMO staged design approach in Europe, *Nucl. Fusion* **59** 066013 (2019). doi:10.1088/1741-4326/ab1178

6 M E Austin *et al*, Achievement of reactor-relevant performance in negative triangularity shape in the DIII-D tokamak, *Phys. Rev. Lett.* **122** 115001 (2019). doi:10.1103/PhysRevLett.122.115001

7 A Marinoni, O Sauter and S Coda, A brief history of negative triangularity tokamak plasmas, *Rev. Mod. Plasma Phys.* **5** 6 (2021). doi:10.1007/s41614-021-00054-0

8 S Hahn *et al*, 45.5-tesla direct-current magnetic field generated with a high-temperature superconducting magnet, *Nature* **570** 496 (2019). doi:10.1038/s41586-019-1293-1

9 S Hahn *et al*, No-insulation multi-width winding technique for high temperature superconducting magnet, *Appl. Phys. Lett.* **103** 173511 (2013). doi:10.1063/1.4826217

10 J L MacManus-Driscoll and S C Wimbush, Processing and application of high-temperature superconducting coated conductors, *Nat. Rev. Mater.* **6** 587 (2021). doi:10.1038/s41578-021-00290-3

11 A Molodyk *et al*, Development and large volume production of extremely high current density $YBa_2Cu_3O_7$ superconducting wires for fusion, *Sci. Rep.* **11** 2084 (2021). doi:10.1038/s41598-021-81559-z

12 D X Fischer *et al*, The effect of fast neutron irradiation on the superconducting properties of REBCO coated conductors, *IEEE Trans. Appl. Supercond.* **28** 8001705 (2018). doi:10.1109/TASC.2018.2807367

13 R Prokopec, D X Fischer, H W Weber and M Eisterer, Suitability of coated conductors for fusion magnets in view of their radiation response, *Supercond. Sci. Technol.* **28** 014005 (2015). doi:10.1088/0953-2048/28/1/014005

14 P K Romano, N E Horelik, B R Herman, A G Nelson, B Forget and K Smith, OpenMC: a state-of-the-art Monte Carlo code for research and development, *Ann. Nucl. Energy* **82** 90 (2015). doi:10.1016/j.anucene.2014.07.048

15 D A Brown *et al*, ENDF/B-VIII.0: the 8th major release of the nuclear reaction data library with CIELO-project cross sections, new standards and thermal scattering data, *Nucl. Data Sheets* **148** 1 (2018). doi:10.1016/j.nds.2018.02.001

16 Fusion Evaluated Nuclear Data Library FENDL-3.2, IAEA Nuclear Data Section, Vienna (2021).

17 A Davis and A Turner, Comparison of global variance reduction techniques for Monte Carlo radiation transport simulations of ITER, *Fusion Eng. Des.* **86** 2698 (2011). doi:10.1016/j.fusengdes.2011.01.059

18 C G Windsor *et al*, Tungsten boride shields in a spherical tokamak fusion power plant, *Nucl. Fusion* **61** 086018 (2021). doi:10.1088/1741-4326/ac09ce

19 C G Windsor *et al*, Shielding materials in the compact spherical tokamak, *Phil. Trans. R. Soc. A* **377** 20170443 (2019). doi:10.1098/rsta.2017.0443

20 M J Norgett, M T Robinson and I M Torrens, A proposed method of calculating displacement dose rates, *Nucl. Eng. Des.* **33** 50 (1975). doi:10.1016/0029-5493(75)90035-7

21 M R Gilbert, S L Dudarev, S Zheng, L W Packer and J-Ch Sublet, An integrated model for materials in a fusion power plant: transmutation, gas production, and helium embrittlement under neutron irradiation, *Nucl. Fusion* **52** 083019 (2012). doi:10.1088/0029-5515/52/8/083019

COLOPHON

How this document was made

The Kronos Fleet — Combined Editorial, 2026 is set in **Fraunces** (display), **Gelasio** (text), and **IBM Plex Mono** (data & equations), carried forward from the Kronos editorial design system.

The figures are rendered at 300 dpi from the deposited generator scripts; the document is composed as a single self-contained file with embedded fonts and imagery, paginated to US Letter, and rendered to PDF through a headless Chromium engine in matched light and dark editions.

Every headline quantity carries an evidence class; withdrawn and restated values are marked as such. Nothing herein is frozen beyond the founder-approved Tier-A set.

Explore it live — turn the interactive 3-D model, run the deposited solvers in the physics validator, and watch the companion film series.

LEGAL NOTICE

Notice, status, and distribution

Conceptual design & simulation study. This document reports a conceptual design and simulation study. It is not a construction commitment, a safety-analysis report, a regulatory filing, or an offer of securities. Forward-looking statements — schedules, costs, market sizes, and performance — are estimates subject to the limitations set out in the Simulations part and may change.

Numbers and their classes. Quantities are reported with evidence classes and case labels; modelled, assumed, and requirement-class values are identified as such and are not to be quoted without their labels.

Public edition. This edition carries the physics and design only; all financial, funding, and defense-commercial content has been removed for public distribution. The scientific text corresponds to the arXiv and journal submissions.

THE 2026 KRONOS SERIES

One programme, many papers

This editorial is one paper in the Kronos 2026 series — a real fusion company's complete, reproducible physics record for a spherical-tokamak breeder and its low-neutron D–^{3}He tandem-mirror burners. Every headline number is a frozen anchor in the Physics De-Risking Register.

Explore the whole programme: the De-Risking Register, the interactive 3-D model, and the physics validator.

KRONOS FUSION ENERGY

The Consumable Centrepost: Coverage-versus-Protection Neutronics, Coil Integrity, and Fused Quench Detection for a Compact Spherical-Tokamak Breeder

A real fusion company building real machines. Explore the science, live.

Zenodo · doi:10.5281/zenodo.22645704

Read on kronosfusionenergy.com

The Physics De-Risking Register